Equilibrium Melting Temperature of Isotactic Polypropylene with High Tacticity: 1. Determination by Differential Scanning Calorimetry

Koji Yamada,*,† Masamichi Hikosaka,‡ Akihiko Toda,‡ Shinichi Yamazaki,‡ and Katsuharu Tagashira†

Kawasaki Development Center, SunAllomer Limited, 2-3-2 Yako, Kawasaki-ku, Kawasaki 210-8548, Japan, and Faculty of Integrated Arts and Sciences, Hiroshima University, 1-7-1 Kagamiyama, Higashi-Hiroshima 739-8521, Japan

Received July 26, 2002; Revised Manuscript Received February 24, 2003

ABSTRACT: A new method to determine the correct Gibbs−Thomson plot and equilibrium melting temperature (T_m^0) of polymers was proposed. The Gibbs−Thomson plot method is reliable, because the Gibbs−Thomson equation is directly derived from thermodynamical relations. In this method, the heating rate dependence of melting temperature (T_m) was omitted by applying the theory of the "melting kinetics", and the effect of lamellar thickening on T_m was also omitted by observing thick lamellae. A differential scanning calorimeter (DSC) was used for observation of T_m as a conventional method. Transmission electron microscope (TEM) was used to observe a distribution of lamellar thickness (l). It was shown theoretically that peak temperature of melting endotherm (T_m(DSC)) corresponded to averaged reciprocal l ($\langle l^{-1}\rangle$) for the case of sharp distributions of T_m and l^{-1}. The Gibbs−Thomson plot, T_m (DSC) vs $\langle l^{-1}\rangle$, was carried out. A reliable Gibbs−Thomson plot and $T_m^0 = 186.2$ °C were obtained for a fraction of isotactic polypropylene (iPP) with high tacticity ([*mmmm*] = 99.6%, $M_n = 64 \times 10^3$ and $M_w/M_n = 2.4$). It was shown that DSC double melting endotherm corresponded to the number-distribution of l^{-1}, when lamellar thickening did not occur.

1. Introduction

The equilibrium melting temperature (T_m^0) is one of the most important basic physical quantities of polymer materials. T_m^0 is also important in study of crystallization mechanism, because crystallization phenomenon, such as lateral growth rate and nucleation rate, is controlled by the degree of supercooling (ΔT), which is defined by $\Delta T \equiv T_m^0 - T_c$, where T_c is crystallization temperature. Determination of T_m^0 has been carried out applying several approaches for long time. [1−13] However, reliable T_m^0s have not been obtained in many polymers yet due to some difficult problems shown below. Therefore, determination of T_m^0 is one of the most important unsolved problems in polymer science.

1.1. Equilibrium Melting Temperature of Polymers. Polymers usually form lamellar crystals. The lamellar thickness (l) of folded chain crystal (FCC) is on the order of several or tens of nanometers and that of extended chain crystal (ECC) reaches to several hundreds of nanometers or a few micrometers.[14−18]

T_m^0 is defined as a melting temperature (T_m) of ideal crystal that has infinite crystal size. Two methods are well-known for the determination of T_m^0 of polymers. One is the Gibbs−Thomson plot method, and another is the Hoffman−Weeks plot method.[1,11]

When we assume a lamellar crystal with lateral sizes a and b and thickness l, the melting temperature (T_m) of lamellar crystal with l ($T_m(l)$) is given by the Gibbs−Thomson equation

$$T_m(l) = T_m^0\left(1 - \frac{2}{\Delta h}\left(\frac{\sigma}{a} + \frac{\sigma}{b} + \frac{\sigma_e}{l}\right)\right) \qquad (1a)$$

where σ is the surface free energy, σ_e is the end surface free energy, and Δh is the heat of fusion.[1] l of ECC of polyethylene (PE) is a few micrometers and a and b are much larger than a few tens of micrometers.[19] Thus, a and b are larger than l in the case of a lamellar crystal. Therefore, eq 1a is approximated by

$$T_m(l) \cong T_m^0 - \frac{C}{l}, \quad \text{where } C = \frac{2\sigma_e T_m^0}{\Delta h} \qquad (1b)$$

The Gibbs−Thomson equation is directly derived from thermodynamical relations, considering the excess free energy by the end surfaces. Therefore, the Gibbs−Thomson equation is correct and reliable. $T_m(l)$ decreases with decrease of l, and so it is a few tens of degrees or several tens of degrees lower than T_m^0 for fcc. Equation 1b shows a linear relationship between $T_m(l)$ and l^{-1}, which is called the Gibbs−Thomson plot. T_m^0 is given by the intercept of $T_m(l)$ at $l^{-1} = 0$

$$\lim_{l\to\infty} T_m(l) = T_m^0 \qquad (2)$$

For example, the Gibbs−Thomson plot has been obtained for fcc and ECC of linear polyethylene (PE).[1,20] In this paper, the Gibbs−Thomson plot method will be applied.

The Hoffman−Weeks plot method is widely used to estimate T_m^0.[2,6,9−11] However, this method is not always reliable. In the succeeding paper (part 2), it will be shown that the Hoffman−Weeks plot is correct under $l \propto 1/\Delta T$.[21]

1.2. Problems in the Gibbs—Thomson Plot of Polymers. I. Effects of "Melting Kinetics" and Lamellar Thickening. It is important to obtain the correct $T_m(l)$ to carry out the reliable Gibbs−Thomson plot. It is well-known that observed T_m (T_m(obs)) of polymer crystals is apparently affected by heating rate (β).[22−27] T_m(obs) increases with increase of β, when

* Corresponding author.
† SunAllomer Ltd.
‡ Hiroshima University.

10.1021/ma021206i CCC: $25.00
Published on Web 06/04/2003

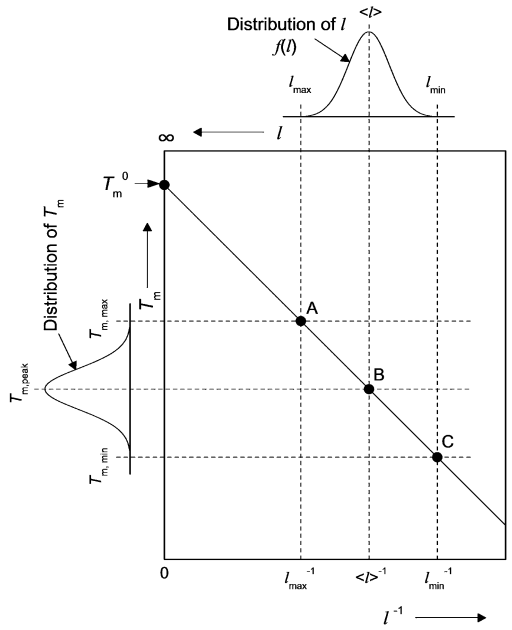

Figure 1. Correspondence between distributions of melting temperature (T_m) and lamellar thickness (l) in the Gibbs−Thomson plot.

lamellar thickening and melt-recrystallization do not occur on heating. The β dependence of T_m(obs) is related to the "melting kinetics", which we proposed as a possible nucleation mechanism of melting in polymer crystallites.[25,26]

T_m(obs) is also affected by lamellar thickening.[28−30] T_m(obs) increases when lamellae thicken on heating. This effect is much more significant for thin lamellae crystallized at lower T_c.

Thus, it is important to omit the two effects of the "melting kinetics" and lamellar thickening from T_m(obs). However, they were not fully omitted in T_m determination in past many studies. In this study, they will be omitted from T_m(obs) in order to obtain correct T_m.

1.3. Problems in the Gibbs—Thomson Plot of Polymers. II. Effect of Distribution of Lamellar Thickness. It is well-known that l of polymer crystals shows distribution.[31] Accordingly, T_m also shows distribution. In this paper, the number-distribution function of lamella with l is denoted by $f(l)$. The correspondence between $f(l)$ and distribution of T_m in the Gibbs−Thomson plot is schematically shown in Figure 1. The upper horizontal axis indicates l. The maximum l (l_{max}), averaged one ($\langle l \rangle$) and the minimum one (l_{min}) correspond to the maximum T_m ($T_{m,max}$), peak of T_m ($T_{m,peak}$) and the minimum T_m ($T_{m,min}$), as indicated by A, B, and C, respectively.

The $f(l)$ is directly obtained by means of transmission electron microscope (TEM), while small-angle X-ray scattering gives a kind of $\langle l \rangle$ and does not give the $f(l)$. Therefore, TEM is the most reliable method for observation of l. In this study, TEM will be used for observation of l.

Differential scanning calorimeter (DSC) is a convenient method to determine T_m. DSC curve shows distribution of T_m. $T_{m,peak}$ is defined as T_m(DSC) in this paper. In the case of sharp DSC profile, T_m(DSC) is nearly equal to averaged T_m ($\langle T_m \rangle$). Therefore, T_m(DSC) should correspond to $\langle l^{-1} \rangle$. Equation 1b is approximated by

$$T_m(\mathrm{DSC}) = T_m{}^0 - C\langle l^{-1} \rangle \qquad (3)$$

In this paper, eq 3 will be used. It will be shown how to obtain $\langle l^{-1} \rangle$ by using $f(l)$ in section 3.

Zhou and Wilkes corresponded mass-based distribution of l to DSC curve by using PE.[31] To our knowledge, no attempt about thus correspondence was made for other polymers. However, they assumed $T_m{}^0$ in order to obtain mass-based distribution of l. Therefore, their method cannot be applied for determination of $T_m{}^0$.

1.4. $T_m{}^0$ of the α2′ Form of Isotactic Polypropylene. Isotactic polypropylene (iPP) is one of the most important polymer materials for commercial application. IPP is also regarded as a typical model of stereoregular polymers. Stereodefects along a molecular chain affect on crystallization and melting behavior. Therefore, stereoregularity should be as high as possible for determination of $T_m{}^0$. IPP fraction with high tacticity (the pentad fraction, $[mmmm] = 99.6\%$) was used in this study.

The α form is conventional for iPP and classified into α1 and α2 form.[32−35] α2 form is observed for high tacticity sample. Recently, we found a new phase, the α2′ phase, at high temperature.[36,37] The α2−α2′ transition reversibly occurs at the transition temperature ($T_{\alpha 2-\alpha 2'}$),

$$T_{\alpha 2-\alpha 2'} = 159\ ^\circ\mathrm{C} \quad (M_n = 64 \times 10^3) \qquad (4)$$

In this paper, it will be shown that T_m of samples crystallized at $T_c \geq 130$ °C is higher than 160 °C which is higher than $T_{\alpha 2-\alpha 2'}$. Therefore, T_m and $T_m{}^0$ can be regarded as those of the α2′ crystal, which is denoted as $T_{m,\alpha 2'}$ and $T_{m,\alpha 2'}{}^0$, respectively.

$T_m{}^0$s of iPP obtained by applying the Gibbs−Thomson plot method are shown in Table 1.[2,3,10] The variation of reported values was several degrees for samples with similar molecular weight and tacticity. However, there were critical problems that effects of the "melting kinetics" and lamellar thickening were not omitted from T_m(obs) in past studies. Purpose of this paper is to obtain $T_{m,\alpha 2'}{}^0$ of iPP.

1.5. Multiple Melting Endotherm of Isotactic Polypropylene in DSC. DSC multiple melting endotherm was studied for long time.[6,9,38−46] It is caused by melt-recrystallization, multiple peaks of $f(l)$, and so on. When T_c is high enough, melt-recrystallization does not occur on heating. Therefore, isothermal crystallization will be carried out at $T_c \geq 148$ °C in this study. It will be shown that multiple melting behavior can be explained by multiple peaks in $f(l)$.

1.6. Purpose of This Study. The purpose of this study is to establish a method to determine the correct $T_m{}^0$ of polymers. Effect of the "melting kinetics" will be omitted from T_m(obs) by applying theory proposed by Toda et al. Effect of lamellar thickening on T_m(obs) will be also omitted by using values of thick lamellae. DSC and TEM will be used to observe T_m and l, respectively. The Gibbs−Thomson plot, T_m(DSC) vs $\langle l^{-1} \rangle$, will be carried out by using well fractioned iPP with high tacticity.

2. How to Obtain the Correct T_m by Omitting Effects of the "Melting Kinetics" and Lamellar Thickening on T_m. (Theory)

2.1. Effect of the "Melting Kinetics" on T_m. Recently, Toda et al. proposed a theory of the "melting kinetics".[25,26] The "melting kinetics" is a concept that the melting should be controlled by diffusion or nucle-

Table 1. T_m^0 of IPP Estimated by Gibbs−Thomson Plots in the Literature

author(s)	T_m^0, °C	method: T_m	method: l	sample
Mezghani and Phillips[10]	186.1	optical microscope	SAXS $\langle l \rangle$	isotacticity > 99%, $M_n = 50 \times 10^3$, $M_w = 151 \times 10^3$, $M_z = 287 \times 10^3$
Cheng et al.[2]	184.4	DSC, onset	SAXS $\langle l \rangle$	$[mmmm] = 98.8\%$, $M_w = 202 \times 10^3$, $M_w/M_n = 2.6$
	183.2	DSC, onset	SAXS $\langle l \rangle$	$[mmmm] = 97.8\%$, $M_w = 159 \times 10^3$, $M_w/M_n = 2.3$
	180.5	DSC, onset	SAXS $\langle l \rangle$	$[mmmm] = 95.3\%$, $M_w = 189 \times 10^3$, $M_w/M_n = 3.0$
Cheng et al.[3]	180.7	DSC, onset	SAXS $\langle l \rangle$	tacticity >99%, $M_n = 15 \times 10^3$, $M_w/M_n = 1.7$
	185.0	DSC, onset	SAXS $\langle l \rangle$	tacticity >99%, $M_n = 300 \times 10^3$, $M_w/M_n = 2.0$

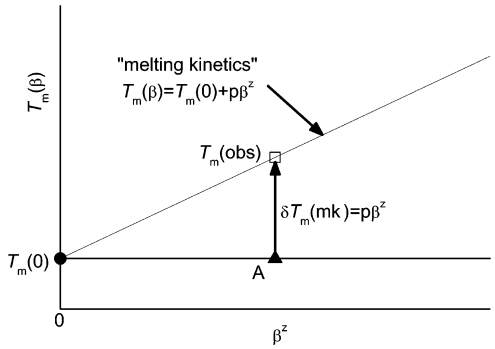

Figure 2. Schematical illustration of effect of "melting kinetics" on T_m. "A" indicates correct T_m at $\beta = 0$ K/min ($T_m(0)$). On heating, the observed T_m (T_m(obs)) linearly increased with increase of β^z.

ation kinetics. They formulated the β dependence of T_m

$$T_m(\text{obs}) = T_m(\beta) = T_m(0) + \delta T_m(\text{mk}) = T_m(0) + p\beta^z \quad (5)$$

where $T_m(\beta)$ is T_m observed at β, $T_m(0)$ is $T_m(\beta)$ observed at $\beta = 0$ K/min, δT_m(mk) indicates an increase of T_m due to the "melting kinetics" and p and z are constants.[25,26] δT_m(mk) is illustrated in Figure 2. T_m(obs) is higher than $T_m(0)$ by δT_m(mk) as indicated by A in Figure 2. The "melting kinetics" can be omitted by

$$T_m(0) = \lim_{\beta \to 0} T_m(\beta) \quad (6)$$

2.2. Effect of Lamellar Thickening on T_m. Fischer et al. and Geil et al. showed that lamellar thickening occurs at high temperature.[44,45] l increased linearly with increase of logarithm of annealing or crystallization time (t) at a constant temperature as shown,

$$l = l^* + W \log t \quad (7)$$

where l^* is l of a critical nucleus and W is thickening rate. The increase of T_m(obs) due to lamellar thickening is denoted as δT_m(lth) in this paper.

The effect of lamellar thickening on T_m(obs) in the Gibbs−Thomson plot is illustrated in Figure 3. The upper axis indicates l. When l increases from l to $l + \delta l$ on heating, the decrease in l^{-1} ($\delta(l^{-1})$) is given by

$$\delta(l^{-1}) = \frac{1}{l} - \frac{1}{l + \delta l} \cong \frac{\delta l}{l^2} \quad (8)$$

Here, $l \gg \delta l$ is assumed. It is obvious that $\delta(l^{-1})$ of thick lamellae (A in Figure 3) is much smaller than that of thin lamellae (B). Therefore, δT_m(lth) of A is too small and can be negligible. l should be large enough to omit δT_m(lth) from T_m(obs). It will be shown that thick lamellae are obtained by isothermal crystallization at

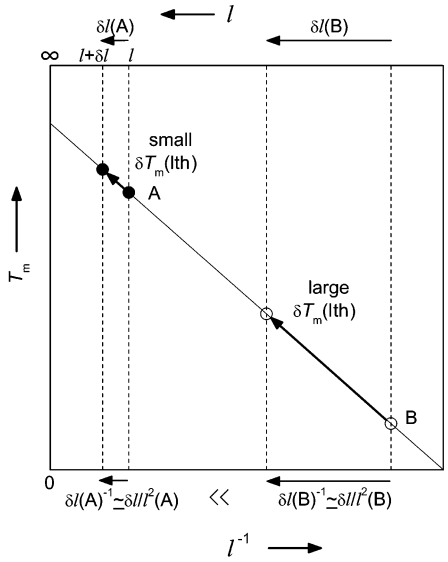

Figure 3. Schematical illustration of effect of lamellar thickening on the Gibbs−Thomson plot. Increases of l and T_m due to lamellar thickening are indicated by δl and δT_m(lth), respectively. δl^{-1} of the thick lamella (A) is larger than that of the thin lamella (B). Therefore, the δT_m(lth) of thick lamella is smaller than that of thin lamella.

high T_c. In this case, l is regarded as a constant on heating,

$$l = \text{constant:} \quad \text{on heating,} \quad T < T_m \quad (9)$$

2.3. Combined Effects of "Melting Kinetics" and Lamellar Thickening on T_m. The combined effects of the "melting kinetics" and lamellar thickening on T_m are illustrated in Figure 4a. Changes of T_m(obs) due to δT_m(mk) and δT_m(lth) are indicated by broken and dotted lines, respectively.

The correct Gibbs−Thomson plot, $T_m(0)$ vs l^{-1}, is shown by a thick line in Figure 4b. In the case of thick lamellae, lamellar thickening does not occur; i.e., $\delta T_m(\text{lth}) \cong 0$. For this case, T_m increases from A0 to T_m(obs) due to the "melting kinetics". In the case of thin lamellae, T_m increases from B0 to B1 and in addition from B1 to T_m(obs) due to the "melting kinetics" and lamellar thickening, respectively.

The smallest l, in which lamellae thickening does not occur, is denoted as l^+. T_m(obs) is given by

$$T_m(\text{obs}) = T_m(0) + \delta T_m(\text{mk}) \quad \text{for } l > l^+ \quad (10a)$$

$$T_m(\text{obs}) = T_m(0) + \delta T_m(\text{lth}) + \delta T_m(\text{mk}) \quad \text{for } l \le l^+ \quad (10b)$$

To obtain correct $T_m(0)$, l should be larger than l^+. In this study, lamellar thickening will be omitted by observing thick lamellae with $l > l^+ = 15$ nm.

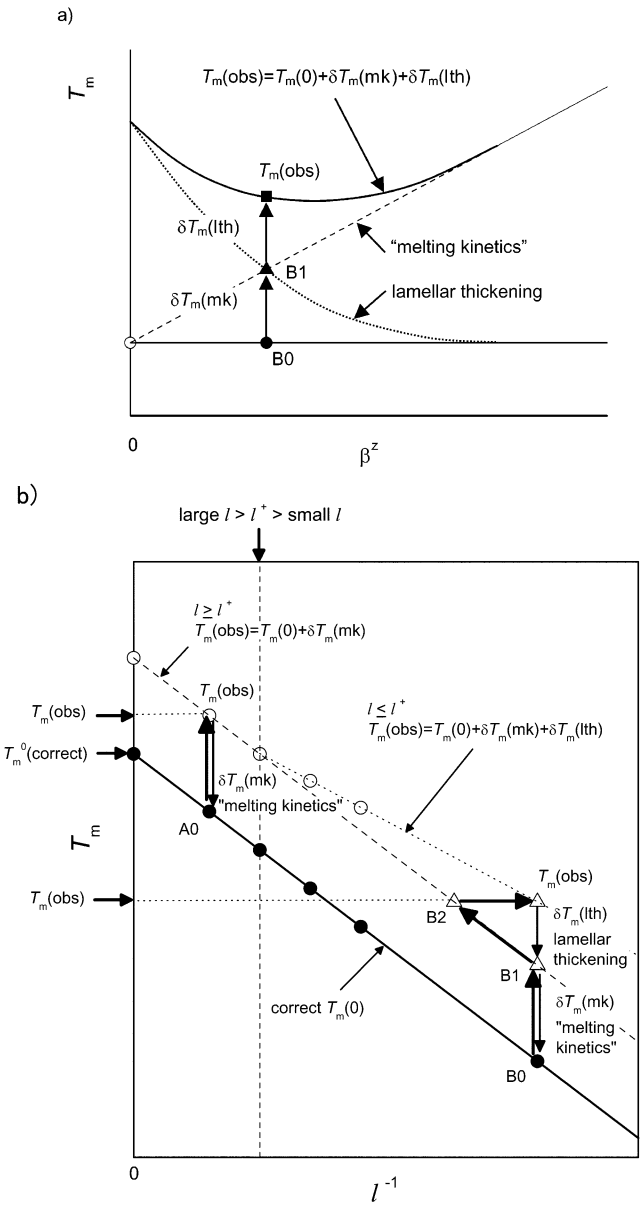

Figure 4. (a) Combined effects of "melting kinetics" and lamellar thickening on T_m. (b) Correction of T_m by omitting the effects of "melting kinetics" and lamellar thickening. l^+ indicates the minimum l where lamellar thickening does not occur. In the case of $l > l^+$, observed T_m (T_m(obs)) is affected by only "melting kinetics". T_m(obs) is higher than correct T_m(0) due to δT_m(mk) (A0). For another case of $l \leq l^+$, T_m(obs) increases due to the "melting kinetics" (δT_m(mk), B0 to B1) and lamellar thickening (δT_m(lth), B1 to B2).

3. Formulation of $\langle l^{-1} \rangle$ (Theory)

The averaged l^{-1} ($\langle l^{-1} \rangle$) approximately corresponds to T_m(DSC) for sharp distributions in l^{-1} and T_m. To determine T_m^0 by applying the Gibbs−Thomson plot, $\langle l^{-1} \rangle$ should be obtained by using the number-distribution of l ($f(l)$). In this section, $\langle l^{-1} \rangle$ will be formulated by theoretical consideration.

3.1. Number-Distribution Function of l ($f(l)$) and Endothermic Distribution of T_m ($\delta H(T_m)$). The $f(l)$ is directly obtained by means of TEM (Figure 5). The DSC curve gives the endothermic distribution function of T_m ($\delta H(T_m)$) and T_m(DSC) (Figure 6).

3.2. Endothermic Distribution of l^{-1} ($\delta H(l^{-1})$) and Averaged l^{-1} ($\langle l^{-1} \rangle$). As is mentioned in section 1.5, melt-recrystallization does not occur when T_c is high enough. In this case, T_m directly corresponds to l^{-1}. Therefore, $\delta H(T_m)$ can be rewritten by the endothermic distribution function of l^{-1} ($\delta H(l^{-1})$) as shown in Figure 6. $\langle l^{-1} \rangle$ is defined by

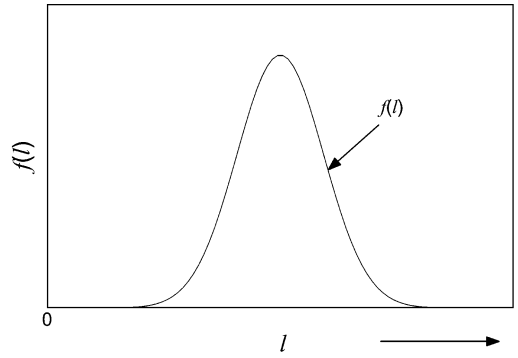

Figure 5. Number-distribution of l ($f(l)$).

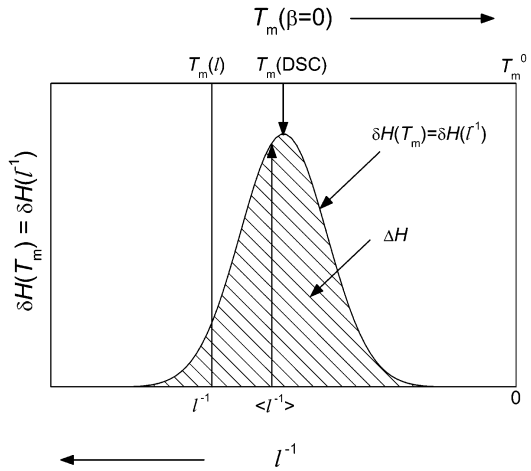

Figure 6. Relation between endothermic distribution function of l^{-1} ($\delta H(l^{-1})$) and that of T_m ($\delta H(T_m)$). $\delta H(l^{-1})$ corresponds to $\delta H(T_m)$, because l^{-1} directly corresponds to T_m in the Gibbs−Thomson equation. Peak of DSC melting endotherm (T_m(DSC)) nearly corresponds to $\langle l^{-1} \rangle$, when DSC curve is rather sharp.

$$\langle l^{-1} \rangle \equiv \frac{\int l^{-1} \delta H(l^{-1})\, \mathrm{d}(l^{-1})}{\int \delta H(l^{-1})\, \mathrm{d}(l^{-1})} \tag{11}$$

The enthalpy of fusion (ΔH) given by the integral of $\delta H(T_m)$ is equal to that given by the integral of $\delta H(l^{-1})$

$$\Delta H = \int_0^\infty \delta H(T_m)\, \mathrm{d}T_m = \int_0^\infty \delta H(l^{-1})\, \mathrm{d}(l^{-1}) \tag{12}$$

3.3. Endothermic Distribution Function of l ($\delta H_l(l)$). We consider a model of lamellae as shown in Figure 7. a and b are lengths of the end surface. The volume-distribution function of l ($\Phi(l)$) is given by

$$\Phi(l) = abl f(l) \tag{13}$$

When the area of the end surface ab is constant for lamellae with different l, $\Phi(l)$ is represented by

$$\Phi(l) \propto l f(l) \tag{14}$$

When lamellae with $\Phi(l)$ melt, the endothermic distribution of l ($\delta H_l(l)$) should be in proportion to $\Phi(l)$ (Figure 8),

$$\delta H_l(l) \propto \Phi(l) \tag{15}$$

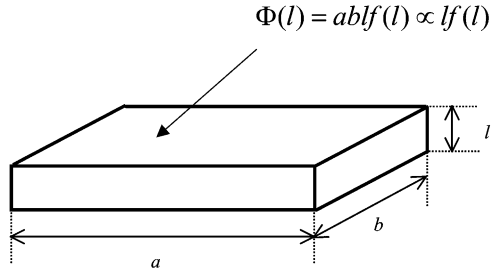

Figure 7. Model of a lamella. The area of end surface, i.e., *a* and *b*, does not depend on *l*.

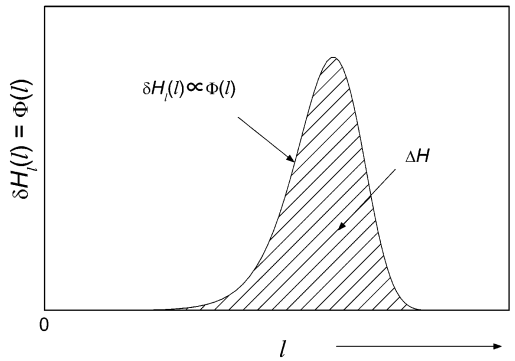

Figure 8. Volume distribution of *l* ($\Phi(l)$), which is proportion to $lf(l)$. $\Phi(l)$ is also proportion to endothermic distribution of *l* ($\delta H_l(l)$).

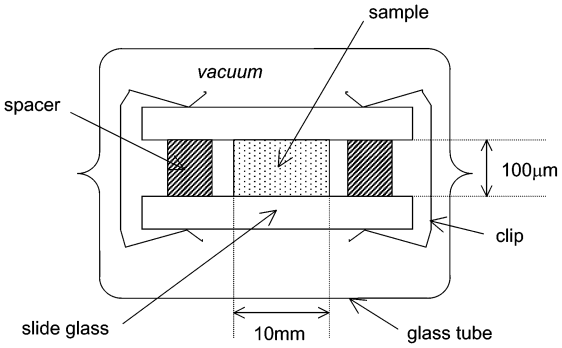

Figure 9. Schematic illustration of the sample assembly.

The combination of eqs 14 and 15 gives

$$\delta H_l(l) \propto lf(l) \tag{16}$$

ΔH is given by the integral of $\delta H_l(l)$,

$$\Delta H = \int_0^\infty \delta H_l(l)\, \mathrm{d}l \tag{17}$$

3.4. Relation between $\delta H(l^{-1})$ and $\delta H_l(l)$. To formulate $\delta H(l^{-1})$ by using $f(l)$, it is necessary to obtain the relation between $\delta H(l^{-1})$ and $\delta H_l(l)$. ΔH given by eq 12 should be equal to that given by eq 17

$$\Delta H = \int_0^\infty \delta H(l^{-1})\, \mathrm{d}(l^{-1}) = \int_0^\infty \delta H_l(l)\, \mathrm{d}l \tag{18}$$

Insertion of eqs 15 and 16 into eq 18 gives

$$\int_0^\infty \frac{\delta H(l^{-1})}{l^2}\, \mathrm{d}l \propto \int_0^\infty lf(l)\, \mathrm{d}l \tag{19}$$

Here, $d(l^{-1}) = -l^{-2}dl$ is used. When $\delta H(l^{-1})$ and $f(l)$ are rather sharp, $\delta H(l^{-1})$ is approximated by

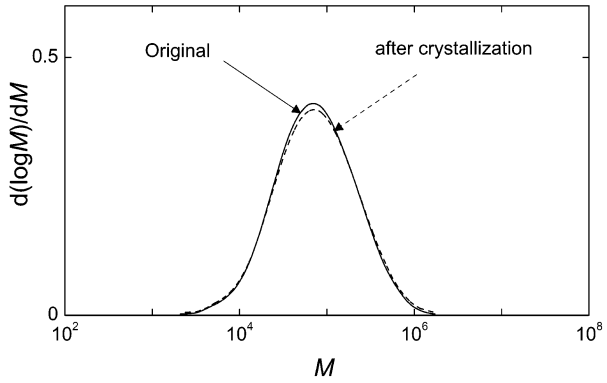

Figure 10. Typical GPC curves of samples before and after crystallization at 160 °C for 1 month.

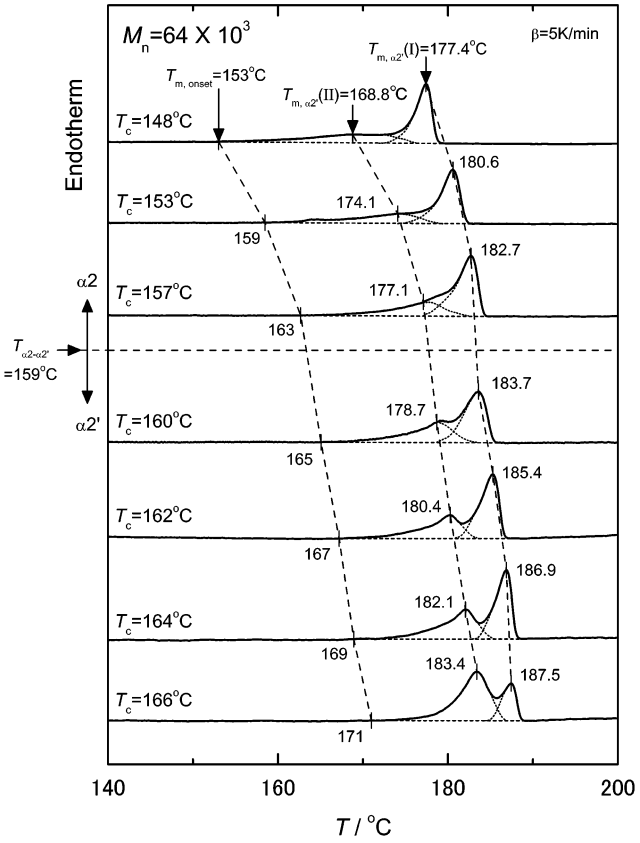

Figure 11. DSC melting curves of samples crystallized at indicated T_cs at heating rate (β) of 5 K/min. $T_{m,onset}$, $T_{m,\alpha2'}$(II), and $T_{m,\alpha2'}$(I) are indicated. The α2−α2′ transition temperature ($T_{\alpha2-\alpha2'}$) is shown by broken line. At $T_c \le T_{\alpha2-\alpha2'} = 159$ °C, iPP crystallizes into α2 form. At $T_c > T_{\alpha2-\alpha2'} = 159$°C, iPP crystallizes into α2′ form.

$$\delta H(l^{-1}) \propto l^3 f(l) \tag{20}$$

3.5. Formula of $\langle l^{-1} \rangle$. Insertion of eq 20 into eq 11 gives the final formula of $\langle l^{-1} \rangle$ as a function of $f(l)$,

$$<l^{-1}> \equiv \frac{\int f(l)\, \mathrm{d}l}{\int lf(l)\, \mathrm{d}l} \tag{21}$$

Meanwhile, the averaged *l* ($\langle l \rangle$) is defined by

$$\langle l \rangle \equiv \frac{\int lf(l)\, \mathrm{d}l}{\int f(l)\, \mathrm{d}l} \tag{22}$$

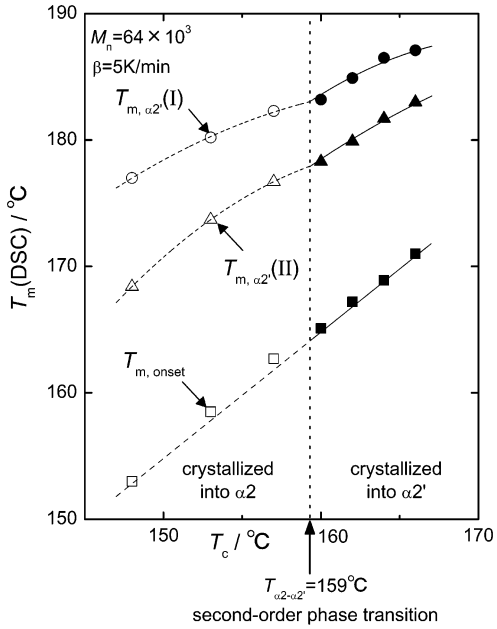

Figure 12. $T_{m,onset}$, $T_{m,\alpha2'}$(II), and $T_{m,\alpha2'}$(I) at $\beta = 5$ K/min were plotted against T_c. $T_c = T_{\alpha2-\alpha2'}$ was indicated by a broken line. Open symbols and filled ones show T_m of samples crystallized into α2 and α2′ phases, respectively.

Therefore, we have a simple relation

$$\langle l^{-1} \rangle \equiv \langle l \rangle^{-1} \tag{23}$$

4. Experimental Section

4.1. Sample. An iPP fraction with high tacticity was used in this study. iPP polymerized by $MgCl_2$-supported catalyst was fractionated by means of the temperature rising elution fractionation method. Molecular weight and molecular weight distribution were measured by means of gel permeation chromatography (GPC), on a Waters 150C, and isotacticity was estimated by ^{13}C nuclear magnetic resonance (NMR) measurements. The obtained characteristics of the iPP fraction were $M_n = 64 \times 10^3$, $M_w = 152 \times 10^3$, $M_w/M_n = 2.4$, and [*mmmm*] = 99.6%. The number of stereodefects was estimated as 1 or 2 per molecule, and a head-to-head sequence was not detected.

4.2. Isothermal Crystallization. Samples were placed between two slide glasses with Cu spacer of 100 μm in thickness within a vacuum glass tube (Figure 9). Samples were melted completely in an oil bath at 220 °C for 10 min and then quickly transferred to another oil bath set to the desired T_c. To obtain thick lamellae, isothermal crystallizations were carried out at higher T_c in comparison with literature for sufficient time to solidify completely, i.e., 148 °C for 18 h, 153 °C for 72 h, 157 °C for 168 h, 160 °C for 672 h, 162 °C for 1464 h, 164 °C for 3660 h, and 166 °C for 4392 h. $T_c = 130$ °C for 1 h and 140 °C for 3 h were also applied in order to confirm the effect of lamellar thickening on T_m. After crystallization, samples were taken out from the oil bath and cooled at room temperature.

4.3. Differential scanning calorimetry. Melting behavior was observed by using a Perkin-Elmer DSC7 under nitrogen flow, 20 mL/min. A small amount of sample, 0.1−2 mg, was cut from the crystallized specimen for DSC measurement. β was changed between 0.2 K/min and 80 K/min.

To discuss the true dependence of melting peak temperature on heating rate (β), we have to evaluate apparent shift due to

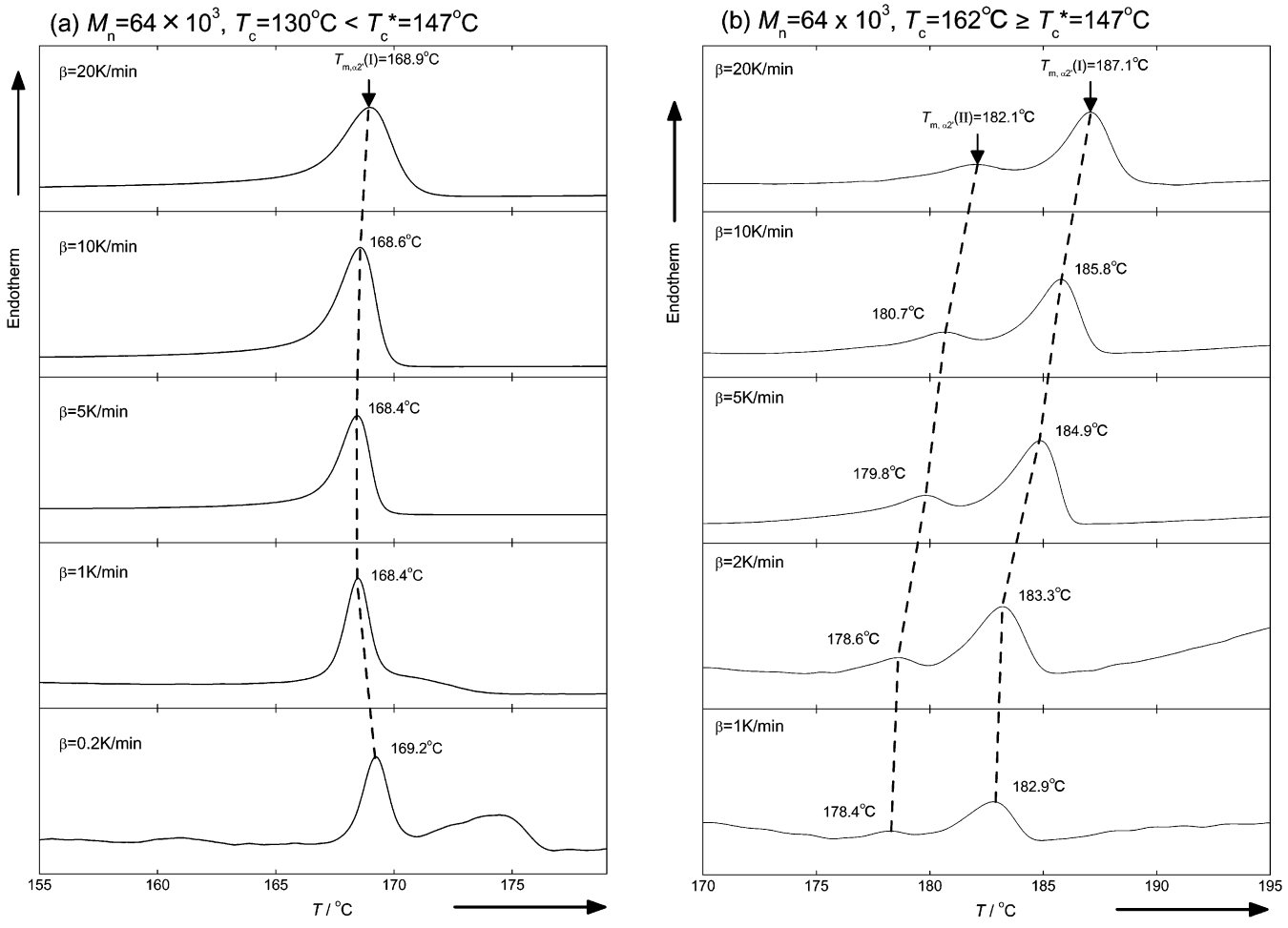

Figure 13. DSC curves at indicated heating rates (β) of samples crystallized at (a) $T_c = 130$ °C and (b) $T_c = 164$ °C.

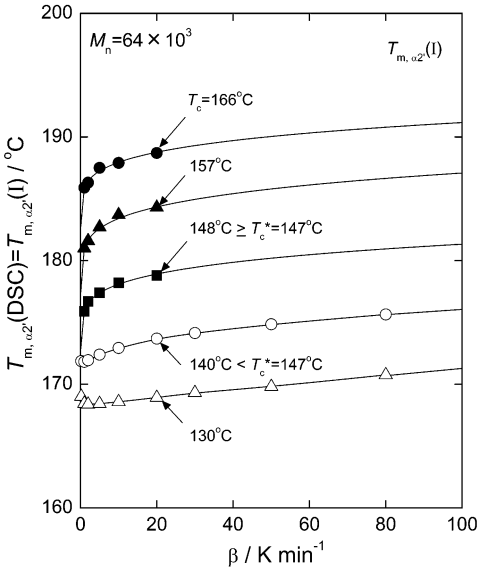

Figure 14. $T_{m,\alpha 2'}$(I)s were plotted against β for samples crystallized at indicated T_c. T_c* (=147 °C) showed the lowest T_c where lamellar thickening does not occur.

instrumental delay by the thermal contact between sample pan and the monitoring station of sample temperature. The conventional method to calibrate the β dependence has been done with the onset temperature of melting of a standard material such as indium. However, it is known that the apparent shift of the peak temperature in the melting region of polymer crystals depends on the peak height and the slope,[46] and hence, the shift cannot be fully calibrated by the conventional method. With a DSC of power compensation type, a calibration method has been proposed with the application of a Laplace transformation, but the procedure is quite complicated[27] because the DSC of power compensation type adjusts the output of a heater placed close to the sample to control the temperature at the monitoring station under the influence of the feedback of sample temperature especially on transition. Therefore, in the present paper, we apply the conventional method as a rough estimate of the apparent shift. The proper calibration method with DSC of heat flux type will be discussed in a separate paper.[26]

4.4. Transmission Electron Microscopy. The lamellar morphology of the ultrathin section was observed by using TEM, HITACHI H-800. Histograms of l and $f(l)$ were obtained from several TEM micrographs different in view. Details of the procedure will be described in part 2 of this series.

5. Results

5.1. Oxidation. A typical example for GPC curves obtained on the samples before and after isothermal crystallization at T_c = 160 °C for 672 h was shown in Figure 10. When crystallization was carried out within a vacuum, molecular weight and its distribution did not change between before and after crystallization. It was concluded that oxidation had not occurred in the ranges of crystallization temperature and time of this study.

5.2. DSC Curves. DSC melting curves of specimens crystallized at T_c = 148−166 °C measured at β = 5 K/min are shown in Figure 11. The baseline was indicated by a broken line. Onset temperature ($T_{m,onset}$) is several degrees higher than T_c. All T_m(DSC)s were higher than 168 °C. At such high temperatures, the induction time of nucleation was longer than a few months. Therefore, so-called melt-recrystallization can-

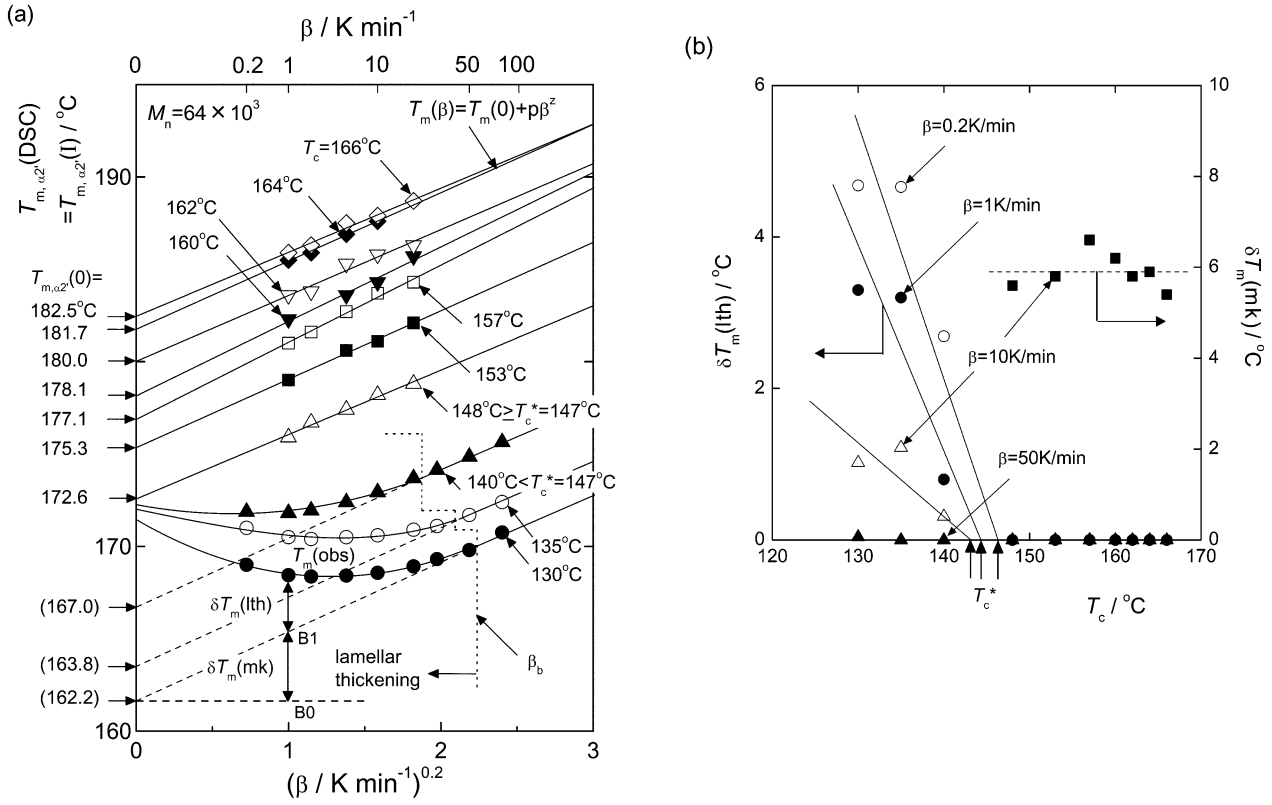

Figure 15. (a) $T_{m,\alpha 2'}$(I)s were plotted against $\beta^{0.2}$ for samples crystallized at different T_cs. $T_{m,\alpha 2'}$(I)s at β = 0 K/min ($T_{m,\alpha 2'}$(0)) were indicated. The broken line indicated the breaking point from linear dependence to the nonlinear one, which was denoted by β_b. At $\beta \leq \beta_b$, lamellae thickening occurred for sample crystallized at $T_c \leq$ 147 °C. Increases of $T_{m,\alpha 2'}$(I) due to the "melting kinetics" and lamellar thickening were shown by δT_m(mk) and δT_m(lth), respectively. (b) Plot of δT_m(lth) against T_c as a function of β.

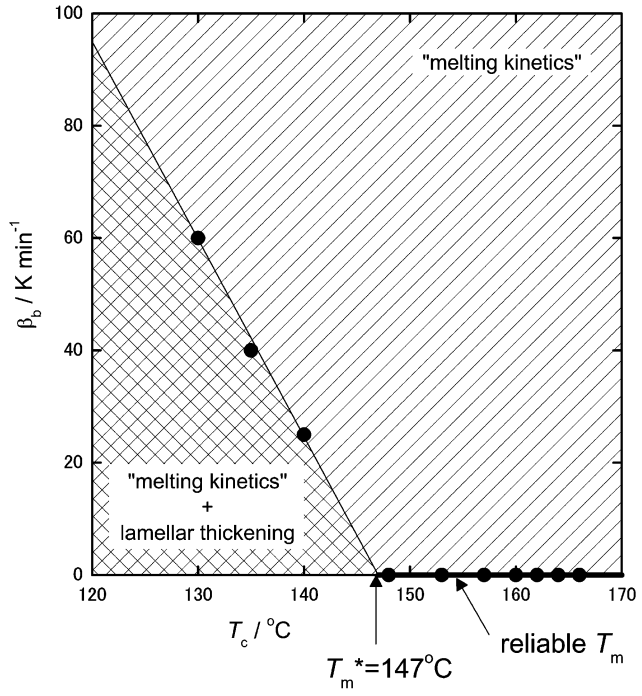

Figure 16. β_b is plotted against T_c. At the right region, only the "melting kinetics" affects on T_m. At the left region, both effects of "melting kinetics" and lamellar thickening on T_m are observed. The thick line indicates that reliable T_m ($T_m(0)$) values can be obtained directly.

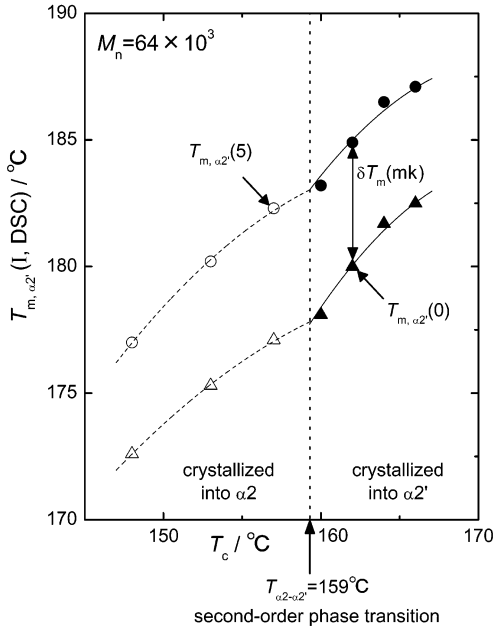

Figure 17. Plot of $T_{m,\alpha2'}$(I) at $\beta = 0$ K/min ($T_{m,\alpha2'}(0)$) vs T_c. $T_{m,\alpha2'}$(I) at $\beta = 5$ K/min ($T_{m,\alpha2'}(5)$) was also plotted. Open symbols and filled ones show T_m of samples crystallized into α2 and α2′ phases, respectively. The difference between $T_{m,\alpha2'}$(0) and $T_{m,\alpha2'}(5)$ is shown by δT_m(mk).

not occur on heating. Double melting endotherms can be separated into two endothermic peaks without any exothermic component for all samples as shown by dotted lines. Peaks at higher and lower temperatures were defined by peak I and peak II, respectively. T_m(DSC)s of peaks I and II were higher than $T_{\alpha2-\alpha2'}$. Therefore, they were denoted as $T_{m,\alpha2'}$(I) and $T_{m,\alpha2'}$(II), respectively.

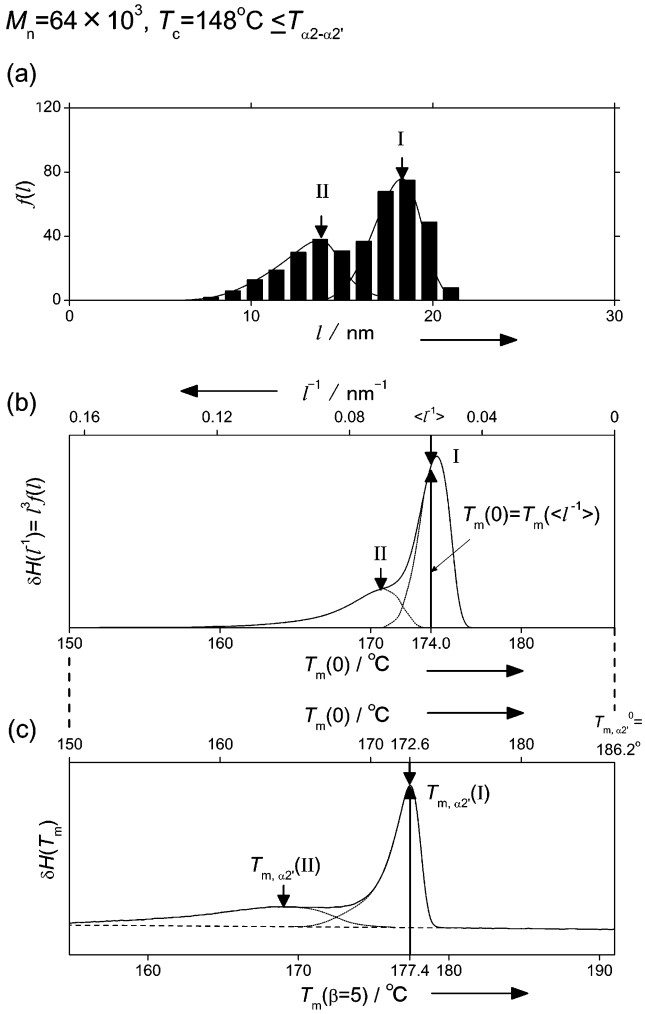

Figure 18. (a) Typical histogram of l of iPP crystallized at T_c = 148 °C ≤ $T_{\alpha2-\alpha2'}$ = 159 °C. Distribution function ($f(l)$) was indicated by solid lines. Peaks I and II of $f(l)$ are indicated. (b) Endothermic distribution of l^{-1} ($\delta H(l^{-1})$), which is equal to $l^3 f(l)$. The upper horizontal axis indicates l^{-1}. The lower axis indicates temperature, which was obtained by using Gibbs−Thomson plot in Figure 20. Peaks I and II are separated from $\delta H(l^{-1})$. $\langle l^{-1}\rangle$ of peak I corresponds to $T_m(0)$ = 172.0 °C. (c) DSC endotherm at β = 5 K/min. The lower axis indicates actual T_m at β = 5 K/min. The upper axis indicates $T_m(0)$ where the effect of the "melting kinetics" was omitted. $T_{m,\alpha2'}$(I) at β = 5 and 0 K/min are 177.0 and 172.6 °C, respectively.

$T_{m,onset}$, $T_{m,\alpha2'}$(II), and $T_{m,\alpha2'}$(I) increased with increase of T_c. The endothermic profile of a sample crystallized at $T_c \le 159$ °C was different from that of a sample crystallized at $T_c > 159$ °C. The T_c = 159 °C corresponds to the α2−α2′ transition temperature ($T_{\alpha2-\alpha2'}$). In the case of $T_c \le T_{\alpha2-\alpha2'}$, broad peak II and sharp peak I were observed. Meanwhile, distinct double peaks were observed for samples crystallized at $T_c > T_{\alpha2-\alpha2'}$. It was concluded that the difference of DSC profile was caused by difference of phases where crystallization occurred.

5.3. T_c Dependence of $T_{m,onset}$, $T_{m,\alpha2'}$(II), and $T_{m,\alpha2'}$(I). $T_{m,onset}$, $T_{m,\alpha2'}$(II), and $T_{m,\alpha2'}$(I) at β = 5 K/min were plotted against T_c (Figure 12). T_ms of samples crystallized into α2 and α2′ were shown by open and filled symbols, respectively. All T_ms increased with increase of T_c. $T_{m,onset}$ was several degrees higher than T_c. Significant increases of $T_{m,\alpha2'}$(II) and $T_{m,\alpha2'}$(I) above $T_{\alpha2-\alpha2'}$ were observed. The differential coefficient

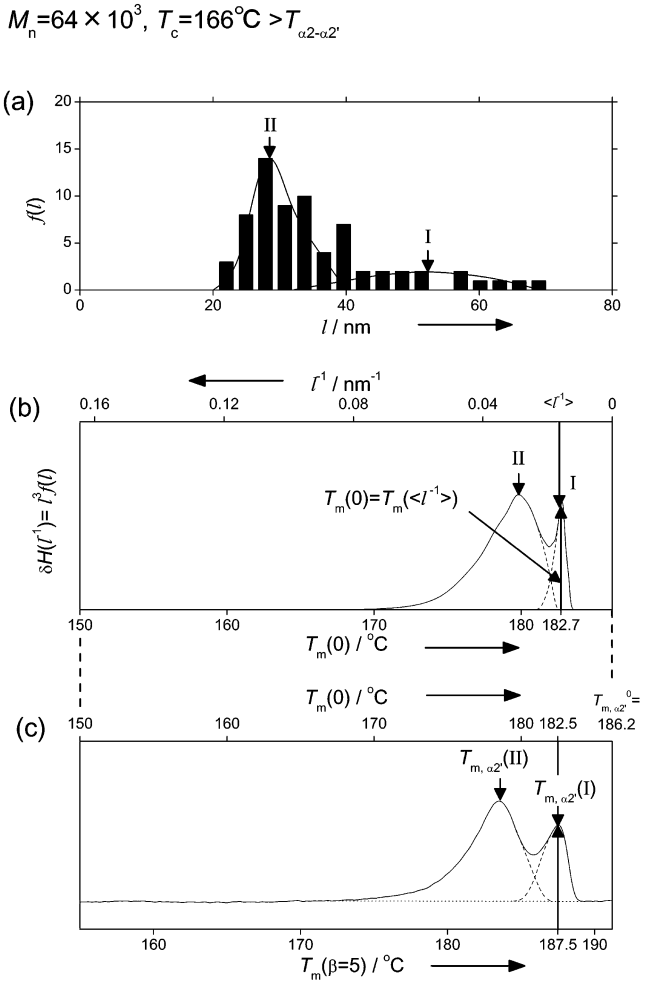

Figure 19. (a) Typical histogram of l of iPP crystallized at T_c = 166 °C > $T_{\alpha2-\alpha2'}$ = 159 °C. Distribution function ($f(l)$) was indicated by solid lines. Peaks I and II are indicated. (b) Endothermic distribution of l^{-1} ($\delta H(l^{-1})$). The upper horizontal axis indicates l^{-1}. The lower axis indicates temperature, which was obtained by using the Gibbs−Thomson plot in Figure 20. Peaks I and II are separated from $\delta H(l^{-1})$. $\langle l^{-1}\rangle$ of peak I corresponds to $T_m(0)$ = 182.0 °C. (c) DSC endotherm at β = 5 K/min. Lower and upper axes indicate T_m at β = 5 K/min and at β = 0 K/min, respectively. $T_{m,\alpha2'}$(I) at β = 5 and 0 K/min are 187.0 and 182.5 °C, respectively.

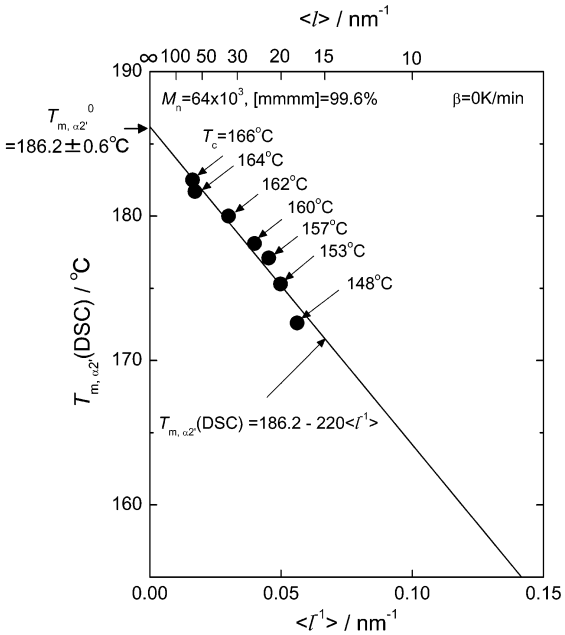

Figure 20. Gibbs−Thomson plot, $T_{m,\alpha2'}$(DSC) vs $\langle l^{-1}\rangle$, of iPP. The upper axis indicates $\langle l\rangle$.

(dT_m/dT_c) of both $T_{m,\alpha2'}$(II) and $T_{m,\alpha2'}$(I) changed at $T_c = T_{\alpha2-\alpha2'}$. The differential coefficients of $T_{m,\alpha2'}$(I) ($dT_{m,\alpha2'}(I)/dT_c$) at T_c = 159 °C were

$$dT_{m,\alpha2'}(I)/dT_c = 0.31, \quad \text{for } T_c \le 159\ °C \quad (24a)$$

$$dT_{m,\alpha2'}(I)/dT_c = 0.81, \quad \text{for } T_c > 159\ °C \quad (24b)$$

Therefore, the breakings of dT_m/dT_c correspond to the α2−α2′ transition and $T_{\alpha2-\alpha2'}$ was obtained by means of DSC ($T_{\alpha2-\alpha2'}$(DSC)),

$$T_{\alpha2-\alpha2'}(\text{DSC}) = 159\ °C \quad (25)$$

5.4. The "Melting Kinetics" and Lamellar Thickening. The β dependence of DSC melting curve changed at T_c = 147 °C that is denoted as T_c*. For a typical example, DSC curves at various β of the sample crystallized at T_c = 130 °C < T_c* = 147 °C are shown in Figure 13a. $T_{m,\alpha2'}$(I) was rather sharp and clearly observed, while $T_{m,\alpha2'}$(II) was very broad and not well observed. At small β (smaller than 5 K/min), $T_{m,\alpha2'}$(I) decreased with increase of β, while at large β (larger than 5 K/min), $T_{m,\alpha2'}$(I) increased with increase of β. In the case of $T_c \ge T_c$* = 147 °C, both $T_{m,\alpha2'}$(I) and $T_{m,\alpha2'}$(II) increased with increase of β in all range (Figure 13b).

To show the effect of β on DSC curve quantitatively, $T_{m,\alpha2'}$(I) was plotted against β as a parameter of T_c in Figure 14. In the case of $T_c < T_c$* = 147 °C, $T_{m,\alpha2'}$(I) decreased with increase of β at small β due to lamellar thickening. After that, it increased with increase of β due to the "melting kinetics". In the case of $T_c \ge T_c$* = 147 °C, $T_{m,\alpha2'}$(I) increased with increase of β for all range of β; i.e., only effect of the "melting kinetics" on T_m was observed and lamellar thickening did not occur at $\beta \cong$ 0.2 K/min.

5.5. Effect of "Melting Kinetics" on T_m. To examine the effect of the "melting kinetics" on T_m, $T_{m,\alpha2'}$(I) was plotted against $\beta^{0.2}$ as a parameter of T_c (Figure 15a). In the case of $T_c \ge T_c$* = 147 °C, $T_{m,\alpha2'}$(I) increased linearly with increase of $\beta^{0.2}$. The slope was almost same for all T_cs. The line shifted to higher temperature with increase of T_c. The slope p was obtained

$$p = 3.7 \pm 1.5, \quad \text{for } T_c \ge T_c* = 147\ °C \quad (26a)$$

Therefore

$$\delta T_m(\text{mk}) = 3.7\beta^{0.2} \quad (26b)$$

was obtained. $T_{m,\alpha2'}(0)$ was obtained from the intercept of $T_{m,\alpha2'}$(I) to β = 0.

In the case of low $T_c < T_c$* = 147 °C, $T_{m,\alpha2'}$(I) decreased to the minimum with increase of $\beta^{0.2}$. After that, it increased linearly with an increase of $\beta^{0.2}$. Thus, $T_m(0)$ is affected by δT_m(mk) and δT_m(lth). These are indicated by B0, B1, and T_m(obs) which corresponds to those in Figure 4b.

The δT_m(mk) and δT_m(lth) were plotted against T_c as a parameter of β (Figure 15b). δT_m(mk) increased with increase of β and did not depend on T_c. δT_m(lth) decreased with increase of T_c and reached 0 °C at T_c*

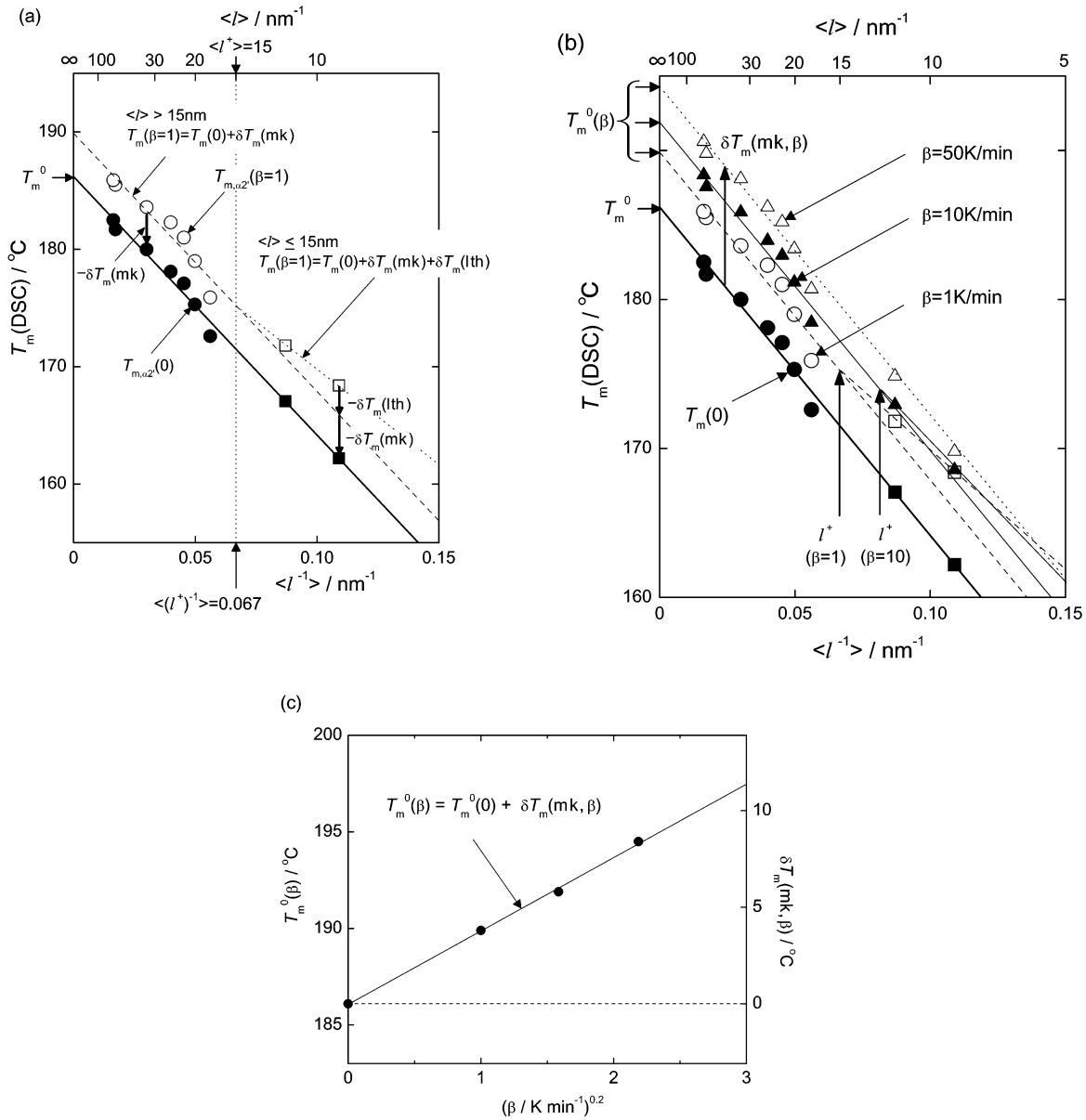

Figure 21. (a) Effects of the "melting kinetics" and lamellar thickening on the Gibbs−Thomson plot. $\langle l^{-1}\rangle$ and $\langle l\rangle$, where the breaking of approximated line was observed, were indicated by $\langle (l^{-1})^{+}\rangle$ and $\langle l^{+}\rangle$, respectively. Open square and dotted line showed T_m affected by lamellar thickening. Open circle and broken line showed T_m affected by the "melting kinetics". (b) Effect of β on the Gibbs−Thomson plot. The Gibbs−Thomson plot shifted upward with increase of β. (c) Plots of $T_m{}^0(\beta)$ and δT_m(lth) vs $\beta^{0.2}$.

= 147 °C. Furthermore, δT_m(lth) decreased and T_c* increased with an increase of β.

The breaking point from linear to nonlinear dependence of $T_{m,\alpha 2'}$(I) on $\beta^{0.2}$ was denoted as β_b. The β_b decreased with increase of T_c and reached $\beta_b = 0$ K/min at T_c* = 147 °C (Figure 16). Therefore, the figure was separated into two regions. The right side is a region where T_m(obs) is affected by only the "melting kinetics". On the left side, both effects were superimposed. It is concluded that the T_m measurement should be carried out for thick lamellae crystallized at $T_c \geq T_c$* = 147 °C, which is indicated by a thick line in Figure 16.

5.6. T_c Dependence of T_m. Correct $T_{m,\alpha 2'}(0)$ values obtained from Figure 15a were plotted against T_c in Figure 17. $T_{m,\alpha 2'}(0)$ increased with increase of T_c. Above 159 °C, the differential coefficient ($dT_{m,\alpha 2'}(0)/dT_c$) was about three times larger than that below 159 °C, which corresponds to the $T_{\alpha 2-\alpha 2'}$. Therefore, it was concluded that the α2−α2′ transition, i.e., solid-to-solid transition, was confirmed by means of DSC.

$T_{m,\alpha 2'}$(I) observed at $\beta = 5$ K/min ($T_{m,\alpha 2'}(\beta = 5)$) was also shown as a reference in Figure 17. It was higher than $T_{m,\alpha 2'}(0)$ due to the "melting kinetics", as indicated by δT_m(mk).

5.7. Number Distribution of *l*, *f*(*l*). Histograms of *l* were obtained from TEM observations (Figures 18a and 19a). The *f*(*l*) was obtained from the histogram. The shape of *f*(*l*) changed between samples crystallized at $T_c \leq T_{\alpha 2-\alpha 2'}$ and those at $T_c > T_{\alpha 2-\alpha 2'}$. Details of lamellar morphology will be shown in the following paper (part 2).

(a) $T_c \leq T_{\alpha 2-\alpha 2'}$. A typical histogram of *l* of a sample crystallized at T_c = 148 °C ≤ $T_{\alpha 2-\alpha 2'}$ is shown in Figure 18a. The range of *l* was 8−20 nm thick. The *f*(*l*) showed bimodal distribution. The two peaks at large and small *l* were denoted as peaks I and II, respectively. The peaks I and II correspond to those of DSC curve, which will be shown in section 5.9.

(b) $T_c > T_{\alpha 2-\alpha 2'}$. Typical histogram of *l* of a sample crystallized at T_c = 166 °C > $T_{\alpha 2-\alpha 2'}$ is shown in Figure

19a. The range of l was 20∼70 nm thick. The $f(l)$ showed a broad bimodal distribution and was separated into two peaks, I and II. The peak I was a very broad one with a wide range of l (30−70 nm) and the maximum l reached 70 nm. On the other hand, the peak II was a rather sharp one with small l (20−40 nm).

5.8. Endothermic-Distribution Function of l^{-1}, $\delta H(l^{-1})$. Endothermic distribution of reciprocal l ($\delta H(l^{-1})$) was obtained from $f(l)$ by using eq 20. Profiles of $\delta H(l^{-1})$ for $T_c \leq T_{\alpha 2-\alpha 2'}$ and $T_c > T_{\alpha 2-\alpha 2'}$ were different as follows.

(a) $T_c \leq T_{\alpha 2-\alpha 2'}$. A typical $\delta H(l^{-1})$ for $T_c = 148$ °C $\leq T_{\alpha 2-\alpha 2'}$ is shown in Figure 18b. The upper horizontal axis indicates l^{-1}. For reference, $T_m(0)$ was added as the lower horizontal axis, which was obtained by applying the Gibbs−Thomson plot in the latter section (Figure 20). $\delta H(l^{-1})$ was separated into two peaks as shown by broken lines. The peaks at smaller and larger l^{-1} were denoted as peak I and II, respectively. Peaks I and II indicated by arrows corresponded to those of $f(l)$, respectively. Peak I was relatively sharp and peak II was very broad. $\langle l^{-1} \rangle$ of peak I was obtained by using eq 21 to be 0.058 nm^{-1}.

(b) $T_c > T_{\alpha 2-\alpha 2'}$. Typical $\delta H(l^{-1})$ for $T_c = 166$ °C > $T_{\alpha 2-\alpha 2'}$ was shown in Figure 19b. It was also separated into two peaks, I and II, which corresponded to those of $f(l)$. Peak I was very sharp and $\langle l^{-1} \rangle$ of peak I was obtained to be 0.017 nm^{-1}.

5.9. Correspondence between the DSC Melting Curve and $\delta H(l^{-1})$. The DSC melting curve should directly correspond to $\delta H(l^{-1})$. Observed DSC curves at $\beta = 5$ K/min for $T_c \leq T_{\alpha 2-\alpha 2'}$ and $T_c > T_{\alpha 2-\alpha 2'}$ are shown in Figure 18c and 19c, respectively.

(a) $T_c \leq T_{\alpha 2-\alpha 2'}$. The DSC curve for $T_c = 148$ °C < $T_{\alpha 2-\alpha 2'}$ is shown in Figure 18c. Lower and upper horizontal axes indicate $T_m(\beta = 5)$ and $T_m(0)$, respectively. The scale of upper horizontal axis directly corresponds to that of the lower horizontal axis of Figure 18b. A sharp peak I and a broad peak II of DSC curve correspond to those in Figure 19b, respectively.

$T_m(0)$ obtained from $\delta H(l^{-1})$ of peak I by applying the Gibbs−Thomson plot in Figure 20 was 172.0 °C. The profile of $\delta H(l^{-1})$ corresponded to that of DSC ($\delta H(T_m)$). $T_{m,\alpha 2'}(0) = 172.6$ °C was obtained from the DSC curve (Figure 18c). Thus, peak I of $\delta H(l^{-1})$ was in agreement with that of $\delta H(T_m)$.

(b) $T_c > T_{\alpha 2-\alpha 2'}$. The DSC curve showed a distinct double peak, i.e., peaks I and II, as shown by broken lines (Figure 19c). $T_{m,\alpha 2'}(0)$ was 182.5 °C. Meanwhile, $T_m(0)$ obtained from $\delta H(l^{-1})$ of peak I was 182.0 °C (Figure 19b). Thus, it was shown that $\delta H(l^{-1})$ corresponded to $\delta H(T_m)$. Therefore, DSC profile can be explained by $\delta H(l^{-1})$. It was concluded that $\langle l^{-1} \rangle$ corresponded to T_m(DSC) correctly.

5.10. Equilibrium Melting Temperature. $T_{m,\alpha 2'}(0)$ obtained in section 5.5 was plotted against $\langle l^{-1} \rangle$ obtained by the above method (Figure 20). $T_{m,\alpha 2'}(0)$ increased linearly with decrease of $\langle l^{-1} \rangle$. The Gibbs−Thomson equation was obtained,

$$T_{m,\alpha 2'}(0) = 186.2 - 220\langle l^{-1} \rangle \text{ (°C)} \qquad (27)$$

Therefore, $T_{m,\alpha 2'}{}^0$ obtained by using DSC ($T_{m,\alpha 2'}{}^0$(DSC)) was determined as

$$T_{m,\alpha 2'}{}^0(\text{DSC}) = 186.2 \pm 0.6 \text{ °C} \qquad (28)$$

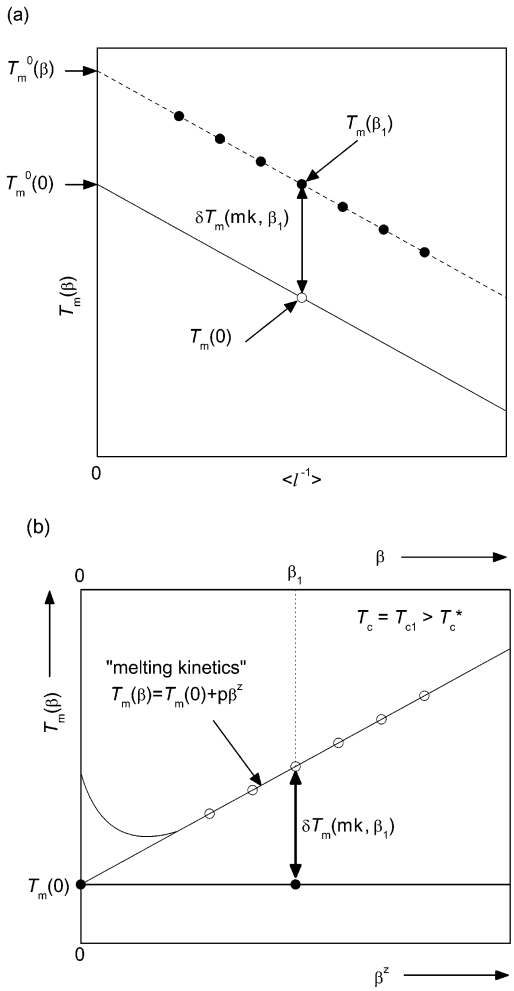

Figure 22. Practical procedure of the Gibbs−Thomson plot. (a) Gibbs−Thomson plot carried out by using $T_m(\beta)$ at $\beta = \beta_1$ ($T_m(\beta_1)$). $\langle l \rangle$ should be larger than $\langle l \rangle^+$ to omit the effect of lamellar thickening. (b) β^z dependence of $T_m(\beta)$. δT_m(mk) depending on β (δT_m(mk, β)) is obtained. For example, at $\beta = \beta_1$, δT_m(mk, β) is denoted by δT_m(mk, β_1). Accordingly, $T_m(0)$ is obtained by subtraction of δT_m(mk, β_1) from $T_m(\beta_1)$.

6. Discussion

6.1. Effect of Heating Rate on the Gibbs−Thomson Plot. It will be shown that the result of the Gibbs−Thomson plot by using $T_m(0)$ can be obtained also from that by using raw data of T_m. T_m(obs) at $\beta = 1$ K/min was plotted against $\langle l^{-1} \rangle$ by open symbols in Figure 21a. The upper axis indicates $\langle l \rangle$. Breaking in the slope of $dT_m(\text{DSC})/d\langle l^{-1} \rangle$ occurred at l^+. δT_m(lth) and δT_m(mk, β), obtained from Figure 15a, were subtracted from T_m(obs). $T_m(0)$ was obtained as shown by filled circles and a solid line. The relation between $T_m(\beta)$ and T_m(obs) is shown by eq 10, parts a and b.

The Gibbs−Thomson plots for $\beta = 1$, 10, and 50 K/min are shown in Figure 21b. The correct $T_m(0)$ at $\beta = 0$ K/min is also shown. δT_m(mk, β) increased with an increase of β. Therefore, $T_m(\beta)$ shifted upward with increase of β. $\langle l^+ \rangle$ decreased with increase of β, because the annealing time decreased with increase of β. $T_m{}^0$ observed at β ($T_m{}^0(\beta)$) was plotted against $\beta^{0.2}$ in Figure 21c. $T_m{}^0(\beta)$ increased linearly with increase of $\beta^{0.2}$. The slope of $T_m{}^0(\beta)$ against $\beta^{0.2}$ is the same as that of $T_m(\beta)$ against $\beta^{0.2}$.

Cheng et al. and Phillips et al. observed thin lamellae smaller than 20 nm, and T_m observations were carried

out at $\beta = 10$ K/min.[2,10] If the δT_m(mk) and δT_m(lth) are omitted from their T_m(obs), the Gibbs−Thomson plots should shift downward and the slopes should be changed. Therefore, their T_m^0 could become lower.

6.2. Practical Procedure of the Gibbs−Thomson Plot. In this section, a practical and convenient procedure to obtain a correct Gibbs−Thomson plot is summarized. In this study, $T_m(0)$s for all T_cs were obtained from Figure 15a.

(1) Raw data of $T_m(\beta)$s at a β ($=\beta_1$) ($T_m(\beta_1)$) are plotted against $\langle l^{-1}\rangle$ for samples crystallized at $T_c > T_c^+$ (Figure 22a). $T_m^0(\beta_1)$ is obtained by the intercept at the vertical axis.

(2) δT_m(mk) at β_1 (δT_m(mk, β_1)) is obtained from the plot of $T_m(\beta)$ vs β^z for only a sample crystallized at one T_c (Figure 22b).

(3) The plot of $T_m(\beta = \beta_1)$ vs l^{-1} shifts downward by δT_m(mk, β_1), and so the plot of $T_m(0)$ vs l^{-1} is obtained as shown by filled circles and a solid line (Figure 22a) because the δT_m(mk, β_1) does not depend on T_c.

(4) The correct T_m^0 is obtained from the intercept at the vertical axis.

In this procedure, isothermal crystallization should be carried out at $T_c > T_c^+$. The correct Gibbs−Thomson plot can be carried out easily by obtaining the plots of $T_m(\beta_1)$ vs $\langle l^{-1}\rangle$ and $T_m(\beta)$ vs β^z.

7. Conclusion

(1) A new method to obtain the correct Gibbs−Thomson plot for T_m^0 was proposed. In this method, the effects of the "melting kinetics" and lamellar thickening should be omitted from T_m.

(2) DSC was used to determine melting temperature (T_m) as a conventional method. l was obtained by means of TEM. It was shown theoretically that the peak of T_m corresponded to averaged reciprocal lamellar thickness ($\langle l^{-1}\rangle$) for sharp distributions of T_m and l^{-1}.

(3) The T_m^0 of iPP was obtained to be 186.2 °C by the plot of $T_{m,\alpha 2'}(0)$ and $\langle l^{-1}\rangle$.

(4) Multiple melting endotherms were observed for iPP. Lamellar thickening and melt-recrystallization did not occur on heating for thick lamellae crystallized at $T_c > 147$ °C. It was shown that the bimodal number-distribution of l^{-1} corresponded to the DSC double endotherm.

Acknowledgment. K.Y. is grateful to Dr. Ian Heritage, the General Manager of the R&D department, SunAllomer Ltd., and Mr. Hideki Tamano, the Manager of Kawasaki Development Center, SunAllomer Ltd., for their help and support.

References and Notes

(1) Wunderlich, B. *Macromolecular Physics*; Academic Press: New York, 1980; Vol. 3, Crystal Melting.
(2) Cheng, S. Z. D.; Janimak, J. J.; Zhang, A.; Hsieh, E. T. *Polymer* **1991**, *32*, 648.
(3) Cheng, S. Z. D.; Janimak, J. J.; Zhang, A. *Macromolecules* **1990**, *23*, 298.
(4) Monasse, B.; Haudin, J. M. *Colloid Polym. Sci.* **1985**, *263*, 822.
(5) Martuscelli, E.; Silvestre, C.; Abate, G. *Polymer* **1982**, *23*, 229.
(6) Samuels, R. J. *J. Polym. Sci., Polym. Phys. Ed.* **1975**, *13*, 1417.
(7) Wang, Y. F.; Lloyd, D. R. *Polymer* **1993**, *34*, 4740.
(8) Bartczak, Z.; Galeski, A. *Polymer* **1990**, *31*, 2027.
(9) Yadav, Y. S.; Jain, P. C. *Polymer* **1986**, *27*, 721.
(10) Mezghani, K.; Campbell, R. A.; Phillips, P. J. *Macromolecules* **1994**, *27*, 997.
(11) Hoffman, J. D.; Weeks, J. J. *J. Res. Natl. Bur. Stand. (U.S.)* **1962**, *66A*, 13.
(12) Marand, H.; Xu, J.; Srinivas, S. *Macromolecules* **1998**, *31*, 8219.
(13) Xu, J.; Srinivas, S.; Marand, H.; Agarwal, P. *Macromolecules* **1998**, *31*, 8230.
(14) Hikosaka, M.; Amano, K.; Rastogi, S.; Keller, A. *J. Mater. Sci.* **2000**, *35*, 5157.
(15) Hikosaka, M. *Polymer* **1987**, *28*, 1257.
(16) Hikosaka, M. *Polymer* **1990**, *31*, 458.
(17) Wundelich, B.; Arawaka, T. *J. Polym. Sci.* **1964**, *2*, 3697.
(18) Keller, A. *Philos. Mag.* **1957**, *2*, 1171.
(19) Hikosaka, M.; Amano, K.; Rastogi, S.; Keller, A. *Macromolecules* **1997**, *30*, 2067.
(20) Okada, M.; Nishi, M.; Takahashi, M.; Matsuda, H.; Toda, A.; Hikosaka, M. *Polymer* **1998**, *39*, 4535.
(21) Part 2 of this series: Yamada, K.; Hikosaka, M.; Toda, A.; Yamazaki, S.; Tagashira, K. *Macromolecules* 2003 *36*, 4802.
(22) Hellmuth, E.; Wunderich, B. *J. Appl. Phys.* **1965**, *36*, 3039.
(23) Schawe, J. E. K.; Strobl, G. R. *Polymer* **1998**, *39*, 3745.
(24) Sohn, S.; Alizadeh, A.; Marand, H. *Polymer* **2000**, *41*, 8879.
(25) Toda, A.; Tomita, C.; Hikosaka, M.; Saruyama, Y. *Polymer* **1998**, *39*, 5093.
(26) Toda, A.; Hikosaka, M.; Yamada, K. *Polymer* **2002**, *43*, 1667.
(27) Zucca, N.; Erriu, G.; Onnis. S.; Zedda, D.; Longoni, A. *Thermochim. Acta*. **2001**, *366*, 15.
(28) Fischer, E. W.; Schnidt, G. F. *Angew. Chem.* **1962**, *74*, 551.
(29) Statton, W. O.; Geil, P. H. *J. Appl. Polym. Sci.* **1960**, *9*, 357.
(30) O'kane, W. J.; Young, R. J.; Ryan, A. J. *J. Macromol. Sci. Phys.* **1995**, *B34*, 427.
(31) Zhou, H.; Wilkes, G. L. *Polymer* **1997**, *38*, 5735.
(32) Natta, G.; Corradini, P. *Nuovo Cim. Suppl.* **1960**, *15*, 1.
(33) Keith, H. D.; Padden, F. J.; Walter, N. M.; Wycoff, M. W. *J. Appl. Phys.* **1959**, *30*, 1485.
(34) Hikosaka, M.; Seto, T. *Polym. J.* **1973**, *5*, 111.
(35) Radhakrishnan, J.; Ichikawa, K.; Yamada, K.; Toda, A.; Hikosaka, M. *Polymer* **1998**, *13*, 2995.
(36) Gu, F.; Hikosaka, M.; Toda, S.; Ghosh, S. K.; Yamazaki, S.; Arakaki, M.; Yamada, K. *Polymer* **2002**, *43*, 1473.
(37) Maiti, P.; Hikosaka, M.; Yamada, K.; Toda, A.; Gu, F. *Macromolecules* **2000**, *33*, 9069.
(38) Alamo, R. G.; Brown, G. M.; Mandelkern, L.; Lehtinen, A.; Paukkeri, R. *Polymer* **1999**, *40*, 3933.
(39) Bodor, C.; Dalcolmo, H. J.; Schroter, O. *Colloid Polym. Sci.* **1989**, *267*, 480.
(40) Al-raheil, I. S.; Qudah, A. M.; Al-share, M. *J. Appl. Polym. Sci.* **1998**, *67*, 1267.
(41) Guerra, G.; Petraccone, V.; Corradini, P.; De Rosa, C.; Napolitano, R.; Pirozzi, B.; Giunchi, G. *J. Polym. Sci., Polym. Phys. Ed.* **1984**, *22*, 1029.
(42) Paukkeri, R.; Lehtinen, A. *Polymer* **1993**, *34*, 4075.
(43) Paukkeri, R.; Lehtinen, A. *Polymer* **1993**, *34*, 4083.
(44) Fischer, E. W.; Schnidt, G. F. *Angew. Chem.* **1962**, *74*, 551.
(45) Statton, W. O.; Geil, P. H. *J. Appl. Polym. Sci.* **1960**, *9*, 357.
(46) Shawe, J. E. K. *Thermochim Acta* **1993**, *229*, 69.

MA021206I